Journal of Solid State Chemistry 184 (2011) 3202–3207

Contents lists available at SciVerse ScienceDirect

Journal of Solid State Chemistry

journal homepage: www.elsevier.com/locate/jssc

Photoelectrochemical water splitting and simultaneous photoelectrocatalytic degradation of organic pollutant on highly smooth and ordered TiO_2 nanotube arrays

Hongjun Wu [a,b], Zhonghai Zhang [b,c,*]

[a] College of Chemistry and Chemical Engineering, Northeast Petroleum University, Daqing 163318, China
[b] Institute of Basic Energy Science and Technology, George Washington University, VA 20147, USA
[c] Graduate School of Science and Engineering for Research, University of Toyama, 3190 Gofuku, Toyama 930-8555, Japan

ARTICLE INFO

Article history:
Received 7 July 2011
Received in revised form
15 September 2011
Accepted 9 October 2011
Available online 15 October 2011

Keywords:
TiO_2 nanotube
Photoelectrochemical water splitting
Photoelectrocatalytic
Methylene blue

ABSTRACT

The photoelectrochemical water splitting and simultaneous photoelectrocatalytic degradation of organic pollutant were achieved on TiO_2 nanotube electrodes with double purposes of environmental protection and renewable energy production under illumination of simulated solar light. The TiO_2 nanotube arrays (TiO_2 NTs) were fabricated by a two-step anodization method. The TiO_2 NTs prepared in two-step anodization process (2-step TiO_2 NTs) showed much better surface smoothness and tube orderliness than TiO_2 NTs prepared in one-step anodization process (1-step TiO_2 NTs). In the photoelectrochemical water splitting and simultaneous photoelectrocatalytic decomposition process, the 2-step TiO_2 NTs electrode showed both highest photo-conversion efficiency of 1.25% and effective photodecomposition efficiency with existing of methylene blue (MB) as sacrificial agent and as pollutant target. Those results implied that the highly ordered nanostructures provided direct pathway and uniform electric field distribution for effective charges transfer, as well as superior capabilities of light harvesting.

1. Introduction

The hydrogen generation by photoelectrochemical water splitting and simultaneous photoelectrocatalytic removal of pollutants in water is a green and environmentally significant process for double purposes of environmental remediation and renewable energy production [1]. Hydrogen is an efficient energy carrier with high energy density and is also environment friendly. Currently, more than 95% of hydrogen is produced by catalytic thermochemical conversion processes, which involve energy losses and the release of greenhouse gases [2]. The utilization of metal oxides for light harvesting and photoelectrochemical water splitting is a promising avenue for sustainable hydrogen production [3–5]. In 1972, Fujishima and Honda first used TiO_2 photoanodes for hydrogen evolution [6]. Metal oxides such as TiO_2 [7–14], ZnO [15–18], WO_3 [19,20], and Fe_2O_3 [21–24] have subsequently been studied by many research groups for developing photoelectrochemical cell devices. For hydrogen generation by photoelectrochemical water splitting, the photoconversion efficiency and stability of photoelectrodes are the key factors. TiO_2 is especially attractive as a photoelectrode because of its high efficiency, chemical and optical stabilities, and environmental and biological compatibilities.

Recently, nanostructuring techniques have been proven useful in enhancing the performance of TiO_2 materials in many fields [25,26]. The approach of architecture controls, especially highly ordered and regular nanostructures, have performed a large enhancement of surface area and formed unique direction and path of the charge carriers through quantum confinement. The ordered nanotubular structures have been considered the most suitable way to increase active surface without an increase of geometric area and fast way to transfer photo-generated electrons [27].

Electrochemical anodization is an efficient and simple way to fabricate TiO_2 nanotube arrays (TiO_2 NTs). Since the first preparation of porous TiO_2 film as reported by Zwilling et al. [28] and the pioneering work by Gong and co-workers [29] for first preparation of TiO_2 NTs by anodization, this method has been extensively developed. It has been reported that the TiO_2 NTs can remarkably increase the efficiency of water splitting and dye-sensitized solar cells [9,30–35]. Schmuki et al. have alternated the morphology of TiO_2 NTs by adjusting anodization conditions to produce smooth [36], bamboo type [37], and double-wall NTs [38].

In this paper, in order to improve the orderliness of the NTs, two steps anodization processes have been used to prepare the

* Corresponding author at: Institute of Basic Energy Science and Technology, George Washington University, VA 20147, USA. Fax: +1 703 726 8256.
E-mail address: zhonghaizhangwill@gmail.com (Z. Zhang).

0022-4596/$ - see front matter © 2011 Elsevier Inc. All rights reserved.
doi:10.1016/j.jssc.2011.10.012

highly smooth and ordered TiO_2 nanotubes (2-step TiO_2 NTs) [39,40]. Compared to the TiO_2 NTs prepared in conventional one step anodization (1-step TiO_2 NTs), the highly ordered structure, surface smoothness and tube orderliness of the 2-step TiO_2 NTs, presented the new possibilities of improving the electron transport, leading to higher photoconversion efficiency and photoelectrocatalytic efficiency. Although our group has reported the 2-TiO_2 NTs can be efficient for photoelectrochemical water splitting [41], to our best knowledge there has been no report of photoelectrochemical water splitting and simultaneous photoelectrocatalytic decomposition of pollutant dye, methylene blue (MB) in aqueous solution on 2-TiO_2 NTs electrode.

2. Experimental

2.1. Materials

Pure titanium foils (99.6% purity, 0.2 mm thick) were purchased from Nilaco Corp., Japan. Ethylene glycol (EG), ammonium fluoride (NH_4F), methylene blue, sodium sulfate and ethanol of analytical grade were obtained from Wako Chemicals (Japan) and used without further purification. All solutions were prepared with doubly distilled deionized water.

2.2. Preparation of TiO_2 NTs

Two-step electrochemical anodizations were used to fabricate the highly smooth and ordered TiO_2 NTs electrode. Prior to anodization, the Ti foils were first degreased by sonicating in ethanol and cold distilled water in turn, followed by drying in pure nitrogen stream. The anodization experiments were carried out in a conventional two-electrode system with Ti foil (25×10 mm^2) as anode and Pt foil (30×20 mm^2) as cathode, respectively, as the scheme shown in the inset of Fig. 1. All electrolytes consisted of 0.3 wt% NH_4F in an aqueous ethylene glycol solution with 2 vol% water. In the first-step anodization, the Ti foil was anodized at 50 V for 1 h, the nanotube layer would grow on the foil surface, then the grown nanotube layer was removed by sonicating in deionized water, and a mirror surface of Ti was exposed. Whereafter, the pretreated Ti was used as anode for the second-step anodization at 50 V for 30 min. The current–time curves obtained during the anodization of 1- and 2-step TiO_2 NTs are shown in Fig. 1. Similar current–time behaviors are observed for both processes. A sharp drop in current behavior is showed in the first stage because of the formation of a barrier oxide layer; this is followed by an increase in current due to oxide layer pitting by the fluoride ions, after which the current reaches a steady value. The current density is higher in the second-step than that in the first-step, which can be explained by the following reasons. First, in the second-step the decrease in current during the first 10 s was less than that in the first-step, which implied that a thinner barrier oxide layer was formed compared to the first-step because of the already existing oxide layer on the Ti before any treatment. The thickness of the barrier oxide layer influences the resistance and consequently the current density of the electrode. Thinner barrier layer in the second step resulted in the higher current density. Second, in the second step, the electric field has a regular distribution because of the highly ordered surface morphology, which also contributed to increasing the current density. After the anodization processes, the samples were cleaned with distilled water and dried off with N_2 gas. The as-anodized TiO_2 NTs depicted amorphous structure and then the phase was converted into anatase through annealing in dry oxygen environment at 450 °C for 1 h with heating and cooling rate of 2 °C/min. For comparison of photoelectrochemical and photoelectrocatalytic activities, the 1-step TiO_2 NTs samples were also prepared with same thickness.

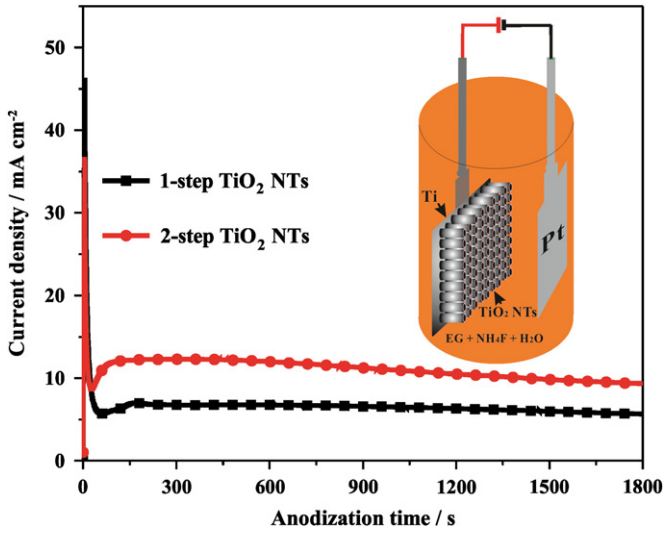

Fig. 1. Variation of anodization current with time for 1- and 2-step TiO_2 NTs. The inset shows the scheme of anodization system.

2.3. Characterization of TiO_2 NTs

The surface morphologies of TiO_2 NTs were characterized by field-emission scanning electron microscopy (FE-SEM) (JEOL, FE-SEM 6700) with accelerated voltage of 5 KeV. The crystalline structures of the TiO_2 NTs were characterized by grazing incidence X-ray diffraction (GIXRD) using a diffractometer with Cu $K\alpha$ radiation (Shimadzu XRD-6000), $\lambda = 0.154$ nm in the range of $2\theta = 20$–70°, with scan rate of 4°/min.

2.4. Photoelectrochemical and photoelectrocatalytic degradation experiments

The photocurrent action spectra were obtained under illumination through a monochromator (SG-80, Yokogawa) in Na_2SO_4 solution with or without MB. The photoelectrochemical water splitting and photoelectrocatalytic degradation experiments were carried out in a pyrex reactor. The samples were illuminated by an artificial sunlight simulator, consisting of a SOLAX lamp (model: SET-140F, SERIC Ltd.) and an AM 1.5 filter (100 mW/cm^2). The TiO_2 NTs electrodes with an active area of 1.0 cm^2 were placed in the reactor as the working electrode, Ag/AgCl in saturated KCl as reference electrode, and platinum foil as counter electrode. All the potentials were referred to Ag/AgCl electrode unless otherwise stated in this paper. In addition, 0.01 M sodium sulfate solution was used as supporting electrolyte. MB aqueous solution with an initial concentration of 1×10^{-6} M was used in the degradation processes, and the pH value of the solution was not controlled during the reaction. All the photoelectrochemical and photoelectrocatalytic experiments were conducted under air condition for general application. The UV–visible absorbance spectra of the MB were measured using a Jasco V-550 UV–vis spectrophotometer, and the concentration of MB solutions were determined by measuring the maximum absorbance at $\lambda = 665$ nm.

3. Results and discussion

The surface morphologies of 1-step TiO_2 NTs and 2-step TiO_2 NTs are shown in Fig. 2. As depicted in the SEM images, the 1-step TiO_2 NTs show a remarkable disparity in length and considerable roughness on the top surface (Fig. 2a and c). The top view of

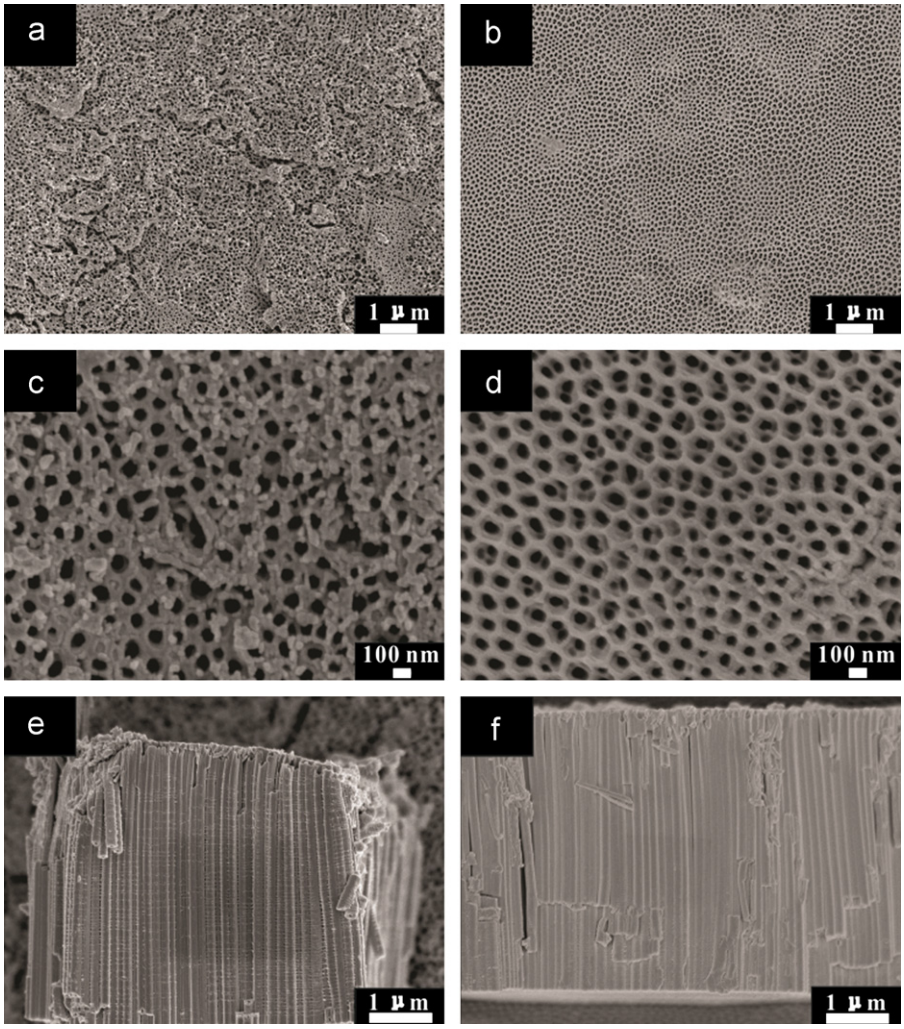

Fig. 2. SEM images of (a and b) top view of 1- and 2-step TiO_2 NTs with a low magnification; (c and d) top view of 1- and 2-step TiO_2 NTs with a high magnification; (e and f) cross-sectional images of 1- and 2-step TiO_2 NTs.

2-step TiO_2 NTs (Fig. 2b and d) present a highly regular and ordered surface with an average diameter of 100 vol%. Fig. 2e shows a cross-sectional image of 1-step TiO_2 NTs indicating ripple-like roughness on the outer walls of the NTs. Cross-sectional image of the 2-step TiO_2 NTs is shown in Fig. 2f with highly smooth NT walls and no ripple-like structure. The NT length of the 1- and 2-step TiO_2 NTs are about 6.0 μm.

GIXRD patterns of 1- and 2-step TiO_2 NTs after annealed and corresponding anatase JCPDS reference pattern are shown in Fig. 3. Both 1- and 2-step TiO_2 NTs exhibit a complete crystallization in the form of anatase phase (JCPDS 21-1272), and show a strong preferential orientation of (101). The 2-step TiO_2 NTs samples showed higher intensity in the (101) pattern than 1-step TiO_2 NTs, which indicated the improvement of the crystallization. The average crystallite sizes (D) of 1- and 2-step TiO_2 NTs were calculated from the width of (101) according to the Debye–Scherrer equation as follows [42]:

$$D = 0.94\lambda/\beta\cos\theta \quad (1)$$

where D is the crystallite dimension, λ is the wavelength of x-ray radiation (Cu $K\alpha = 0.15406$ vol%), θ is the diffraction angle, and β is the corrected peak width at half-maximum intensity (FWHM), the value of β is corrected using the formula $\beta = \beta_m - \beta_{ins}$, where β_m is

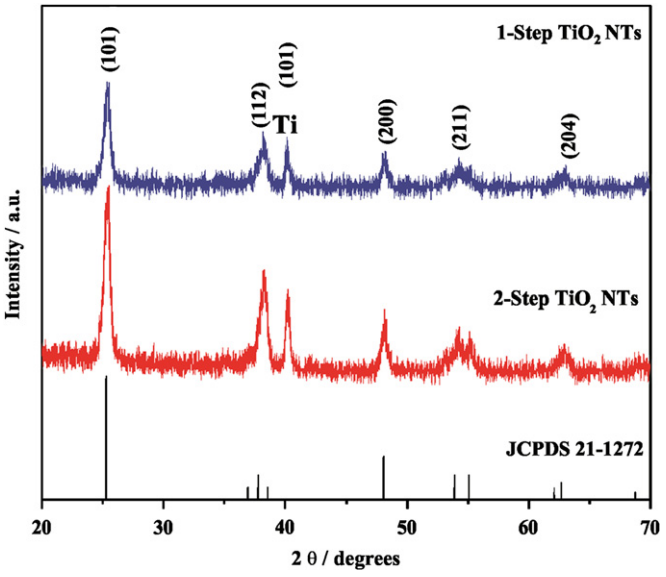

Fig. 3. GIXRD patterns of 1- and 2-step TiO_2 NTs after annealing and corresponding anatase JCPDS reference pattern.

the measured peak width and β_{ins} is the instrumental broadening. According to Eq. (1), the mean crystallite sizes are 18.11 and 18.59 vol% for 1- and 2-step TiO_2 NTs, respectively. The crystallite size is an important factor to determine the stability of TiO_2 NTs crystalline phases. A smaller crystallite size implies more stability for the anatase phase [43].

In order to estimate the quantitative correlation of light absorption on TiO_2 NTs, incident-photon–to–current-conversion efficiency (IPCE) measurements were performed to study the photoresponse wavelength region for 1- and 2-step TiO_2 NTs in Na_2SO_4 with or without MB, as shown in Fig. 4. IPCE can be calculated using the following equation [44]:

$$IPCE = (1240J_p)/(\lambda I_{light}) \quad (2)$$

where J_p is the photocurrent density, λ is the incident light wavelength, and I_{light} is the measured irradiance. The 1- and 2-step TiO_2 NTs behaved in a similar manner, but the 2-step TiO_2 NTs showed the highest IPCE value with existing of MB. The 1-step TiO_2 NTs shows a maximum IPCE value of 20.33% and 15.12% with and without MB, respectively, at 350 vol%. The 2-step TiO_2 NTs shows a maximum IPCE value of 64.8% and 34.8% with or without MB, respectively, at 350 vol%. The higher IPCE value of 2-TiO_2 NTs than that of 1-step TiO_2 NTs implied better light harvesting capacity and faster electrons transfer rate. The increase of IPCE value was observed on both 1- and 2-step TiO_2 NTs with existing of MB. These results implied the restraining of charge recombination for the oxidation of MB with the excited holes on TiO_2 NTs.

Several photoelectrochemical measurements were carried out to evaluate the water splitting on 1- and 2-step TiO_2 NTs with or without MB. Fig. 5a shows a set of linear sweep voltammagrams (LSV) in dark and under illumination of simulated solar light (AM 1.5, 100 mW/cm^2). In dark, the current is insignificant in the range of 10^{-6} A/cm^2 even at a potential of up to 1.0 V, which implied that no electrochemical oxidation occurred. Under illumination, a significant increase of current was observed on both 1- and 2-step TiO_2 NTs. The photocurrent density on 1- and 2-step TiO_2 NTs with or without MB was recorded on 0 V versus Ag/AgCl reference electrode and summarized in Table 1. With existing of MB, the photocurrent density increased up to 29.5% and 46.2% on 1- and 2-step TiO_2 NTs, respectively. The 2-step TiO_2 NTs showed higher photocurrent density with or without MB than 1-step TiO_2 NTs. This indicated that the photogenerated electrons on the

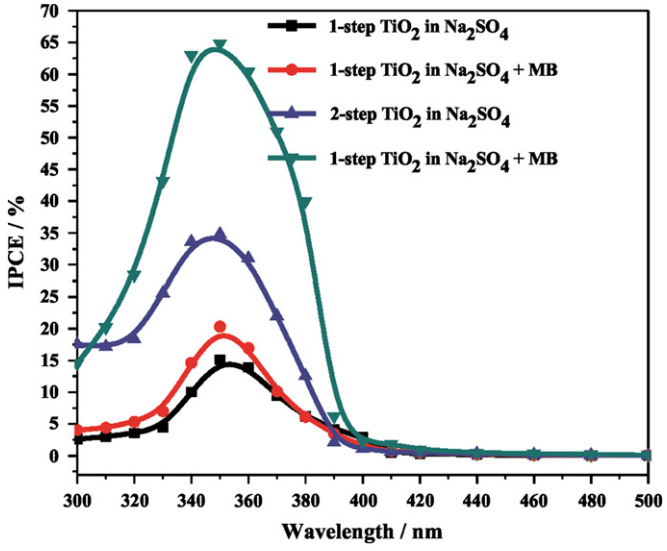

Fig. 4. IPCE analysis of 1- and 2-step TiO_2 NTs in Na_2SO_4 solution with or without MB.

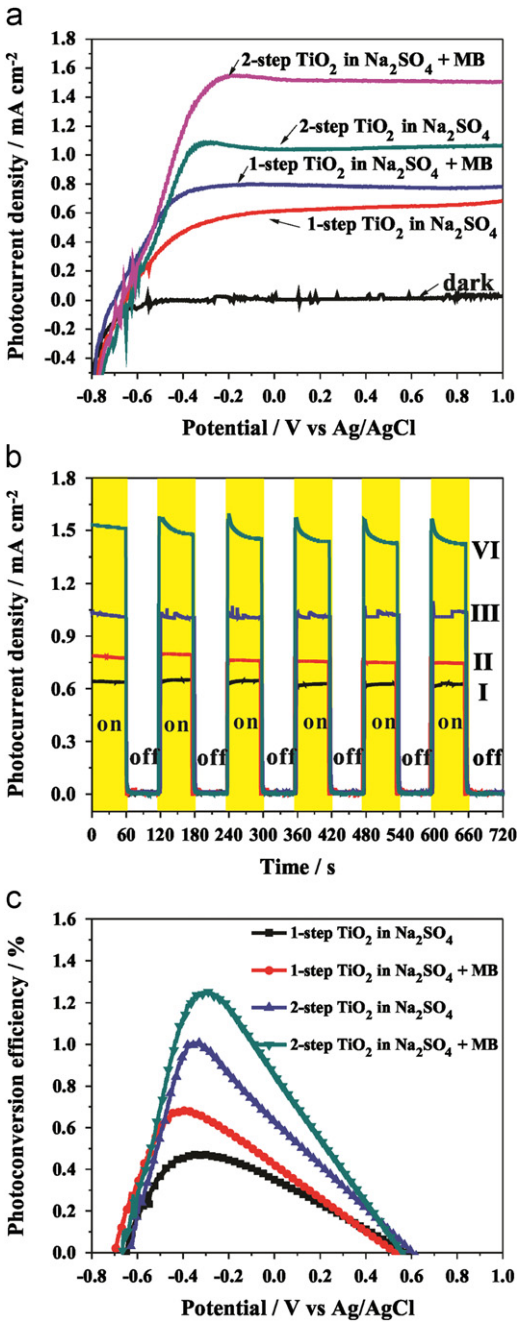

Fig. 5. (a) Linear sweep voltammagrams, collected at a scan rate of 5 mV/s at applied potentials from −0.8 to +1.0 V from 1- and 2-step TiO_2 NTs electrodes in dark and under illumination of 100 mW/cm^2; (b) amperometric I–t curves of the 1- and 2-step TiO_2 NTs at an applied potential of 0 V with 60 s light on/off cycles; (c) photoconversion efficiency as a function of applied potential.

Table 1
Photocurrent Density and Photoconversion Efficiency on 1- and 2-step TiO_2 NTs with or without MB.

	1-step TiO_2 in Na_2SO_4	1-step TiO_2 in Na_2SO_4+MB	2-step TiO_2 in Na_2SO_4	2-step TiO_2 in Na_2SO_4+MB
Photocurrent density (mA/cm^2)	0.61	0.79	1.04	1.52
Photoconversion efficiency (%)	0.472	0.681	1.01	1.25

2-step TiO_2 NTs could be faster transported to the counter electrode, and higher water splitting efficiency could be expected. Amperometric *I–t* measurements were carried out to examine the photoresponse over time. As shown in Fig. 5b, fast photoresponses are recorded both on 1- and 2-step TiO_2 NTs under conditions of light on and off, and those photocucrrent patterns are highly reproducible for numerous on–off cycles.

The photoconversion efficiency for hydrogen generation is calculated via the following equation [45]:

$$\eta(\%) = j_p[(E^{\circ}_{rev} - |E_{app}|)/I_{light}]100 \quad (3)$$

where η is the photoconversion efficiency, j_p is the photocurrent density (mA cm^{-2}), I_{light} is the incident light irradiance, E°_{rev} is the standard reversible potential which is 1.23 V, and E_{app} is the applied potential $E_{app}=E_{meas}-E_{aoc}$, where E_{meas} is the electrode potential of the working electrode and E_{aoc} is the electrode potential of the same working electrode under open circuit condition under illumination. Plots of photoconversion efficiency versus applied potential are shown in Fig. 5c, and the values of efficiency are summarized in Table 1.

The photoelectrocatalytic performance of TiO_2 NTs was evaluated by degradation of MB in aqueous solution. The MB removal on 1- and 2-step TiO_2 NTs electrodes in various degradation processes, photoelectrocatalysis (PEC), photocatalysis (PC), electrochemical oxidation (EO), and direct photolysis (DP), were summarized in Fig. 6a. Applied bias potential in photoelectrocatalysis and electrochemical oxidation processes was 0.6 V. The removal in direct photolysis process was insignificant, which proved that MB was stable under illumination. The result of electrochemical oxidation was also in good agreement with the data in Fig. 5a, where the electrochemical oxidation did not occur evidently in this process. Both on 1- and 2-step TiO_2 NTs electrodes, the photoelectrocatalytic processes provided higher powerful way to degrade the MB, and the latter electrodes, with ordered nanostructures, showed faster degradation efficiency. The experimental data of Fig. 6a were found to fit approximately a pseudo-first-order kinetic model by the linear transforms $\ln(C_0/C)=f(t)=kt$ (k is reaction constant) as shown in Fig. 6b. The values of the reaction constant, k, are shown in Fig. 6c. The reaction constant of 2-step TiO_2 NTs in photoelectrocatalytic process (0.0221 min^{-1}) is 45% higher than that of 1-step TiO_2 NTs in same process (0.0152 min^{-1}). The stability of a photoelectrode was also important to its practical application for organic pollutants degradation. As shown in Fig. 6d, after five times continuous runs for MB degradation, the 2-step TiO_2 NTs electrodes did not exhibit any significant loss of activity under illumination of simulated solar light. This good repetition of degradation results was also verified by photocurrent, which changed little, indicating potential application for environmental remediation.

4. Conclusion

In summary, we prepared highly smooth and ordered TiO_2 NTs by two-step anodization method. The smoothness and orderliness of the 2-TiO_2 NTs were improved considerably in comparison with that of 1-step TiO_2 NTs. The higher photoconversion efficiency for hydrogen generation and degradation efficiency of MB in photoelectrocatalytic process implied that the 2-step TiO_2 NTs was a much better photocatalyst than 1-step TiO_2 NTs, which could be explained by the efficient way of electron transfer due to the highly ordered structures.

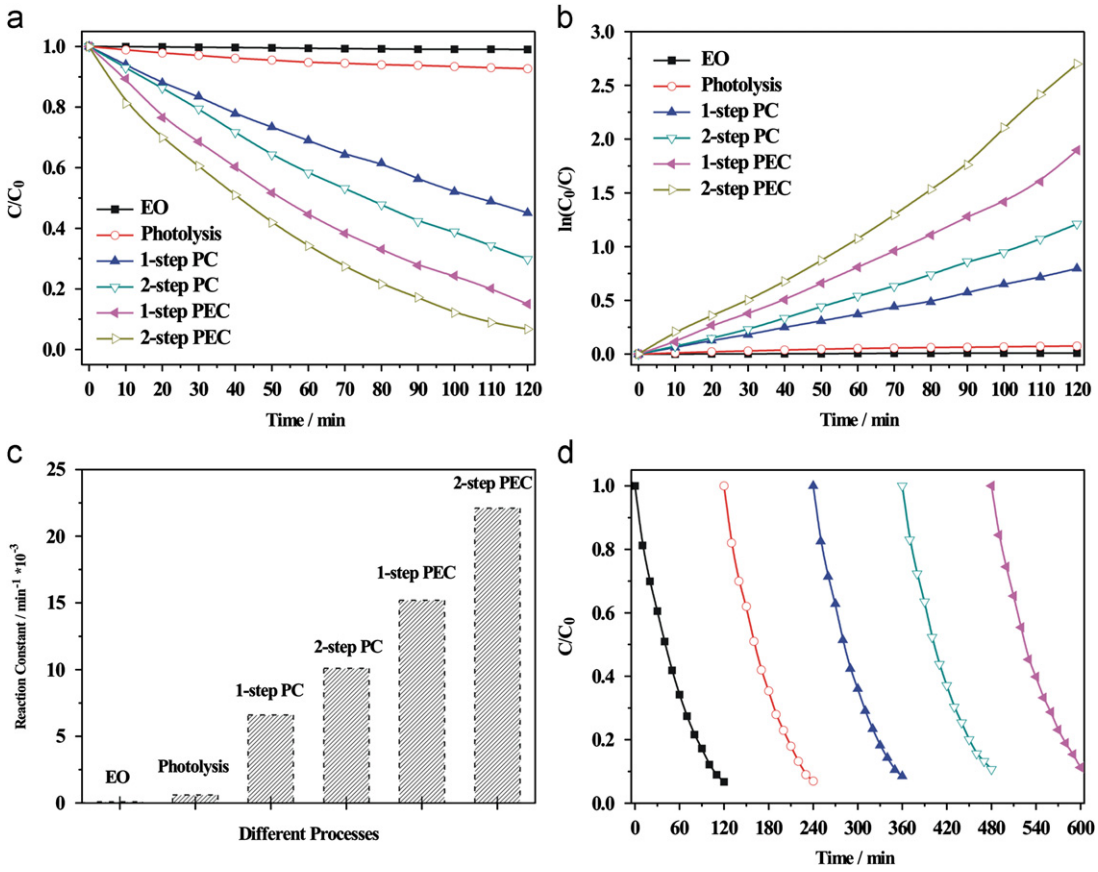

Fig. 6. (a) Photoelectrocatalysis (PEC), photocatalysis (PC), electrochemical oxidation (EO), and direct photolysis (DP) processes on MB degradation, (b) the kinetics of MB removal in different processes; (c) comparison of the corresponding reaction constant (min^{-1}); and (d) stability of 2-step TiO_2 NTs electrode.

References

[1] V.M. Daskalaki, M. Antoniadou, G.L. Puma, D.I. Kondarides, P. Lianos, Environ. Sci. Technol. 44 (2010) 7200–7205.
[2] J.J. Ohi, Mater. Res. 20 (2005) 3167–3179.
[3] M. Gratzel, Nature 414 (2001) 338–344.
[4] A. Kudo, Y. Miseki, Chem. Soc. Rev. 38 (2009) 253–278.
[5] H.G. Park, J.K. Holt, Energy Environ. Sci. 3 (2010) 1028–1036.
[6] A. Fujishima, K. Honda, Nature 238 (1972) 37–38.
[7] A. Fujishima, T.N. Tao, D.A. Tryk., J. Photochem. Photobiol. C 1 (2000) 1–21.
[8] X.B. Chen, S.S. Mao, Chem. Rev. 7 (2007) 2891–2959.
[9] C. Ampelli, G. Centi, R. Passalacqua, S. Perathoner, Energy Environ. Sci. 3 (2010) 292–301.
[10] Z.H. Zhang, Y. Yuan, Y.J. Fang, L.H. Liang, H.C. Ding, G.Y. Shi, L.T. Jin, J. Electroanal. Chem. 610 (2007) 179–185.
[11] J.G. Yu, B. Wang, Appl. Catal. B: Environ. 94 (2010) 295–302.
[12] H.M. Zhang, P.R. Liu, X.L. Liu, S.Q. Zhang, X.D. Yao, T.C. An, R. Amal, H.J. Zhao, Langmuir 26 (2010) 11226–11232.
[13] H.T. Yu, S. Chen, X. Quan, H.M. Zhao, Y.B. Zhang, Appl. Catal. B: Environ. 90 (2009) 242–248.
[14] N. Lu, S. Chen, H.T. Wang, X. Quan, H.M. Zhao, J. Solid State Chem. 181 (2008) 2852–2858.
[15] X.Y. Yang, A. Wolcott, G.M. Wang, A. Sobo, R.C. Fitzmorris, F. Qian, J.Z. Zhang, Y. Li, Nano Lett. 9 (2009) 2331–2336.
[16] M. Guo, P. Diao, X.D. Wang, S.M. Cai, J. Solid State Chem. 178 (2005) 3210–3215.
[17] A. Wolcott, W.A. Smith, T.R. Kuykendall, Y.P. Zhao, J.Z. Zhang, Adv. Func. Mater. 19 (2009) 1849–1856.
[18] M. Guo, P. Diao, S.M. Cai, Appl. Surf. Sci. 249 (2005) 71–75.
[19] L. Weinhardt, M. Blum, M. Bar, C. Heske, B. Cole, B. Marsen, E.L. Miller, J. Phys. Chem. C 112 (2008) 3078–3082.
[20] S.J. Hong, H. Jun, P.H. Borse, J.S. Lee, Int. J. Hydrogen Energy 34 (2009) 3234–3242.
[21] Z.H. Zhang, M.F. Hossain, T. Takahashi, Appl. Catal. B: Environ. 95 (2010) 423–429.
[22] S.K. Mohapatra, S.E. John, S. Banejee, M. Misra, Chem. Mater. 21 (2009) 3048–3055.
[23] J. Brillet, M. Gratzel, K. Sivula, Nano Lett. 10 (2010) 4155–4160.
[24] I. Cesar, A. Kay, J.A.G. Martinez, M. Gratzel, J. Am. Chem. Soc. 128 (2006) 4582–4583.
[25] K. Shankar, J.I. Basham, N.K. Allam, O.K. Varghese, G.K. Mor, X.J. Feng, M. Paulose, J.A. Seabold, K.S. Choi, C.A. Grimes, J. Phys. Chem. C 113 (2009) 6327–6359.
[26] S. Saremi-Yarahmadi, U.K.G. Wijayantha, A.A. Tahir, B. Vaidhyanathan, J. Phys. Chem. C 113 (2009) 4768–4778.
[27] Z.H. Zhang, Y. Yuan, G.Y. Shi, Y.J. Fang, L.H. Liang, H.C. Ding, L.T. Jin., Environ. Sci. Technol. 41 (2007) 6259–6263.
[28] V. Zwilling, E. Darque-Ceretti, A. Boutry-Forveille, D. David, M.Y. Perrin, M. Aucouturier, Surf. Interface. Anal. 27 (1999) 629–637.
[29] D. Gong, C.A. Grimes, O.K. Varghese, J. Mater. Res. 16 (2001) 3331–3334.
[30] N.K. Allam, M.A. El-Sayed, J. Phys. Chem. C 114 (2010) 12024–12029.
[31] K. Zhu, N.R. Neal, A.F. Halverson, J.Y. Kim, A.J. Frank, J. Phys. Chem. C 114 (2010) 13433–13441.
[32] O.K. Varghese, M. Paulose, C.A. Grimes, Nat. Nanotechnol. 4 (2009) 592–597.
[33] C. Richter, C.A. Schmuttenmaer, Nat. Nanotechnol. 5 (2010) 769–772.
[34] S. Sharma, O.K. Varghese, G.K. Mor, T.J. LaTempa, N.K. Allam, C.A. Grimes, J. Mater. Chem. 19 (2009) 3895–3898.
[35] S.E. John, S.K. Mohapatra, M. Misra, Langmuir 25 (2009) 8240–8247.
[36] J.M. Macak, H. Tsuchiya, L. Taveira, S. Aldabergerova, P. Schmuki, Angew. Chem. Int. Ed. 44 (2005) 7463–7465.
[37] S.P. Albu, D. Kim, P. Schmuki, Angew. Chem. Int. Ed. 47 (2008) 1916–1919.
[38] S.P. Albu, A. Ghicov, S. Aldabergenova, P. Drechsel, D. LeClere, G.E. Thompson, J.M. Macak, P. Schmuki, Adv. Mater. 20 (2008) 4135–4139.
[39] S.Q. Li, G.M. Zhang, D.Z. Guo, L.G. Yu, W. Zhang, J. Phys. Chem. C 113 (2009) 12759–12765.
[40] Y. Shin, S. Lee, Nano Lett. 8 (2008) 3171–3173.
[41] Z.H. Zhang, M.F. Hossain, T. Takahashi, Int. J. Hydrogen Energy 35 (2010) 8528–8535.
[42] B.D. Cullity, Elements of X-ray Diffraction, 2nd ed, Addison-Wesley, Reading, MA, 1978, p. 283.
[43] L. Korosi, I. Gekany, Colloids. Surf. A 28 (2006) 146–154.
[44] K. Shankar, G.K. Mor, A. Fitzgerald, C.A. Grimes, J. Phys. Chem. C 111 (2007) 21–26.
[45] B. Parkinson, Acc. Chem. Res. 17 (1984) 431–437.